Differential Cross Section Measurement of Charged Current ν_e Interactions Without Pions in MicroBooNE

MICROBOONE-NOTE-1109-PUB

MicroBooNE Collaboration*

(Dated: May 24, 2022)

This note presents the first measurement of an exclusive electron neutrino cross section with the MicroBooNE experiment using data from the booster neutrino beamline at Fermilab. This measurement is made for a selection of electron neutrinos without pions in the final state, and differential cross sections are extracted in energy and angle with respect to the beam for the electron and the leading proton. The differential cross section as a function of proton energy is measured using events with protons both above and below the visibility threshold. This is done by including a separate selection of electron neutrino events without reconstructed proton candidates in addition to those with proton candidates. Results are compared to the predictions from several modern generators, and good agreement is found between data and these models. The data shows best agreement, as quantified by p-value, with the generators that predict a lower overall cross section, such as GENIE v3 and NuWro.

* microboone_info@fnal.gov

Experiments used for neutrino measurements ranging from measuring the CP phase in the neutrino sector, to addressing long standing experimental anomalies, also address broader physics goals like searching for dark matter particles in the beam, and characterizing supernova explosions [1]. In many of these searches, electron neutrino (ν_e) events constitute either the signal or a dominant background to new physics. It is therefore vital to improve the modeling of ν_e interactions to enable those searches with high sensitivity. MicroBooNE has recently completed the first round of searches [2–5] for an excess of low-energy ν_e events that could explain the MiniBooNE anomaly [6], and did not observe an excess. The search for ν_e events without visible pions [3], however, found some hints of discrepancy with the nominal ν_e model. Compatibility was found to be at the 10-20% level in terms of p-values after systematic uncertainties are constrained with a measurement of high-statistics ν_μ from the same beam, and a qualitative description of the phase space where the tension is larger was provided. In this note we reinterpret this result in terms of a cross section measurement, under the assumption of no new physics, with the goal of providing input to model comparisons and generator tuning.

We present a measurement of ν_e events without final-state pions, and select ν_e events both with and without visible protons. This analysis is the first ν_e-argon cross section measurement in an exclusive final state that can begin to break the degeneracy between models and provide additional discrimination relative to previous inclusive measurements. Also, as a first ν_e cross section measurement on the Booster Neutrino Beamline (BNB) [7], we provide a complementary result to previous measurements [8–10] performed on ν_e events from the NuMI beamline [11].

The MicroBooNE detector [12] is a liquid argon time projection chamber (TPC) experiment and collects data in the BNB at Fermilab. The TPC is a 2.56 m by 2.32 m by 10.36 m volume filled with 85 metric tons of liquid argon. As charged particles travel in the detector they ionize the argon, and the ionization electrons drift in the applied electric field of 273 V/cm, to be collected on three planes of wires. Each plane of wires has a different orientation (vertical, +60 degrees, -60 degrees), so that when they are read out they result in three different "views", which can be combined into 3D images of a neutrino interaction.

The detector also contains a light collection system, consisting of 32 photomultiplier tubes with fast timing resolution, that makes it possible to select charge coincident with the beam timing. The neutrinos measured in this analysis come from the BNB. The neutrinos produced in this beam have an average energy of about 0.8 GeV and are primarily muon neutrinos, with 0.5% electron neutrinos [13]. This analysis measures these intrinsic electron neutrinos using data collected from 2016-2018, corresponding to 6.86×10^{20} protons on target (POT).

The neutrino flux simulation used in this analysis was developed by the MiniBooNE collaboration [13], and modified to use the position of the MicroBooNE detector which is slightly closer to the beam target than MiniBooNE. Neutrino interactions in the detector argon are simulated using v3.0.6 G18_10a_02_11a of the GENIE event generator [14] with the MicroBooNE tune applied [15].

There are several steps involved to simulate the detector response. Particles are propagated through the detector using Geant4 [16], and then the charge and light produced by these particles is simulated with LArSoft [17]. A simulation of the charge induced by drifting electrons is used for the wire and readout electronics response [18, 19], and a look-up table from Geant4 simulation of photon propagation is used to model the production of scintillation light. Data driven electric field maps are used to take into account distortions in the electric field from space charge [20, 21]. A modified box model is used to simulate ion recombination [22], and a time dependent simulation is used for the drift electron lifetime and wire response. Cosmic-rays are a significant background in MicroBooNE, and are incorporated in a data-driven way by overlaying a simulated neutrino interaction onto cosmic data collected during periods of time when the neutrino beam was off. This method also provides a data-driven incorporation of any detector noise.

Neutrino events are reconstructed in this analysis using the Pandora pattern recognition toolkit [23]. A set of algorithms first removes obvious crossing cosmic-rays and then selects a neutrino candidate in time with the beam. Particles are reconstructed as showers or tracks within this neutrino candidate; typically electrons and photons are shower-like, while muons, charged pions, and protons are track-like. The Pandora event reconstruction has been used for many previously published results by the MicroBooNE collaboration [3, 9, 10, 24–31]. Additional tools are used on top of the Pandora pattern recognition, particularly to enhance shower-track separation, perform track particle identification (PID) to separate protons and muons [32], and to perform electron-photon separation [3]. Track and shower energies are measured separately. Calorimetric energy reconstruction is performed for electromagnetic showers, starting with the total energy clustered in the shower (E_{shower}). This is corrected to account for inefficiencies in charge collection using a simulation of electrons, and with this correction the reconstructed energy is defined as E_{reco}=E_{shower}/0.83. For tracks, the energy is estimated based on particle range [33]. Using simulation, the energy resolution is estimated to be 3% for protons, if their kinetic energy is greater than 50 MeV, and 12% for electrons. The absolute resolution on $\cos\theta$ is 0.01 for electrons and 0.03 for protons, where θ is the angle of the particle with respect to the beam.

We define signal events as charged current (CC) ν_e interactions, that contain an outgoing electron with kinetic energy $\text{KE}_e > 30$ MeV, no final-state neutral pions, and no final-state charged pions with $\text{KE}_{\pi^\pm} > 40$ MeV. Signal events are further characterized in terms of the leading proton kinetic energy. Events with visible protons ($\text{KE}_{p,\text{lead}} \geq 50$ MeV)

are defined as $1e\mathrm{N}p0\pi$ events. Events without visible protons ($\mathrm{KE}_{p,\mathrm{lead}} < 50$ MeV), or in which no proton exits the nucleus, are defined as $1e0p0\pi$ events and are required to pass additional phase space restrictions $E_e > 0.5$ GeV and $\cos\theta_e > 0.6$.

We perform a differential cross section measurement in four kinematic variables: the electron energy, the electron angle with respect to the beam, the leading proton energy, and the leading proton angle with respect to the beam. All of these variables except the leading proton energy are measured for only the $1e\mathrm{N}p0\pi$ signal. The leading proton energy is measured for both $1e0p0\pi$ and $1e\mathrm{N}p0\pi$ events with smearing allowed between these two samples. This is the first measurement to characterize proton production in neutrino interactions across the visibility threshold. Using the MicroBooNE tune of GENIE v3 [15], $1e\mathrm{N}p0\pi$ events are predicted to be 60% quasi-elastic (QE) neutrino interactions, 30% meson exchange current (MEC), with subdominant resonant (RES) (10%) and deep inelastic scattering (DIS) (1%) contributions; $1e0p0\pi$ events are mostly QE, with contributions from MEC and RES each at the 10-15% level. The relative abundance of the different interaction types is not flat with respect to the measured variables, which may provide some insight into the differences between models when data is compared to event generators.

Events are selected with separate criteria based on the presence or absence of candidate protons. This selection strategy is the same as [3], although a few of the requirements have been updated to optimize the selections for a cross section measurement. The main objective is to maintain sufficient ν_e purity for a cross section extraction while maximizing the ν_e efficiency across the phase space of the measurement. For both the $1e\mathrm{N}p0\pi$ and $1e0p0\pi$ selections the largest increase in efficiency comes from a relaxed cut on the boosted decision trees (BDTs) used in the analysis. These BDTs are the same, including the training, as those used in [3]. Additionally, for the $1e\mathrm{N}p0\pi$ selection we relax the cuts on proton vs muon particle identification, on the shower $\mathrm{d}E/\mathrm{d}x$, and on the shower conversion distance. For the $1e0p0\pi$ selection we add requirements to increase the purity as needed for a cross section measurement, particularly on the electron candidate $\mathrm{d}E/\mathrm{d}x$, and by restricting the phase space to the highest purity region with $\cos\theta_{\mathrm{e}}^{\mathrm{reco}} > 0.6$ and $\mathrm{E}_{\mathrm{e}}^{\mathrm{reco}} > 0.51$ GeV. We find that with these selections an appropriate visibility threshold for the leading proton kinetic energy is 50 MeV, which is approximately where the $1e0p0\pi$ selection efficiency turns off and the $1e\mathrm{N}p0\pi$ efficiency turns on. Therefore, for $1e\mathrm{N}p0\pi$ selected events we also require that the leading reconstructed proton has $\mathrm{KE}_{p,\mathrm{lead}}^{\mathrm{reco}} > 50$ MeV. With the data sample used in this analysis, a total of 145.5 events are predicted in the $1e\mathrm{N}p0\pi$ selection, with a $1e\mathrm{N}p0\pi$ purity of 69%. We expect to select about 100 (2) true $1e\mathrm{N}p0\pi$ ($1e0p0\pi$) events with an efficiency of 17%. The largest backgrounds to the $1e\mathrm{N}p0\pi$ selection are events with final state π^0 (ν_e CC and ν_μ CC or NC interactions), other ν_μ CC events, and cosmic-rays. In the $1e0p0\pi$ selection about 11 (2) true $1e0p0\pi$ ($1e\mathrm{N}p0\pi$) signal events are predicted with an efficiency of 12% and $1e0p0\pi$ purity of 65%; the total prediction is 17.6 events, and the largest background is from $\mathrm{NC}\pi^0$ events. Using these selections we are able to select events from the subdominant (0.5%) electron neutrino component of the BNB, while removing most of the backgrounds from muon neutrinos and cosmic rays.

The prediction on the total number of selected events is subject to uncertainties from several sources. Variations in the flux prediction may come from uncertainties on the hadron production cross section and on the modeling of the beamline. These are propagated to an uncertainty on the predicted event rate by re-weighting the nominal simulation, and are found to be at the 6% level and relatively flat in terms of the variables used in the analysis. Uncertainties on the neutrino interaction model are included based on the nominal tuned GENIE v3 simulation using a re-weighting method for most of the sources and with a limited set of specific variations [15]. When computing the interaction model uncertainties the true number of signal events is not varied as it is the quantity of interest for the cross section measurement. The impact of these uncertainties is only evaluated on the efficiency and smearing, and they combine to a 4% uncertainty on the total event prediction. Uncertainties on the propagation of final state particles in the detector are assessed by varying re-interaction cross sections for charged pions and protons, again by re-weighting the nominal simulation [34]. These uncertainties are generally at the 1% level, but grow to as high as 8% at high proton energies. Uncertainties on detector modeling are assessed using dedicated samples that are produced by varying parameters related to specific detector effects to amounts compatible with estimates from MicroBooNE data. These include space charge effects, electron-ion recombination, light measurement, and wire response [35]. Overall, these effects combine to a ∼5% effect but can grow to 10-20% at high electron and proton energy as well as for the $1e0p0\pi$ selection. Other subdominant uncertainties are due to the size of simulated samples, the POT measurement, and the estimate of the total number of argon nuclei in the detector. Covariance matrix formalism is used to include systematic uncertainties in the analysis, where the covariance matrix C is defined as:

$$\begin{aligned} C^{\mathrm{Syst}} = \; & C^{\mathrm{Flux}} + C^{\mathrm{XSec}} + C^{\mathrm{Reint}} + \\ & C^{\mathrm{Detector}} + C^{\mathrm{MCstat}} + C^{\mathrm{POT}} + C^{\mathrm{Nnuclei}} \end{aligned}$$

$$C_{ij} = \frac{1}{N}\sum_{k=1}^{N}\left(n_i^k - n_i^{\mathrm{CV}}\right)\left(n_j^k - n_j^{\mathrm{CV}}\right).$$

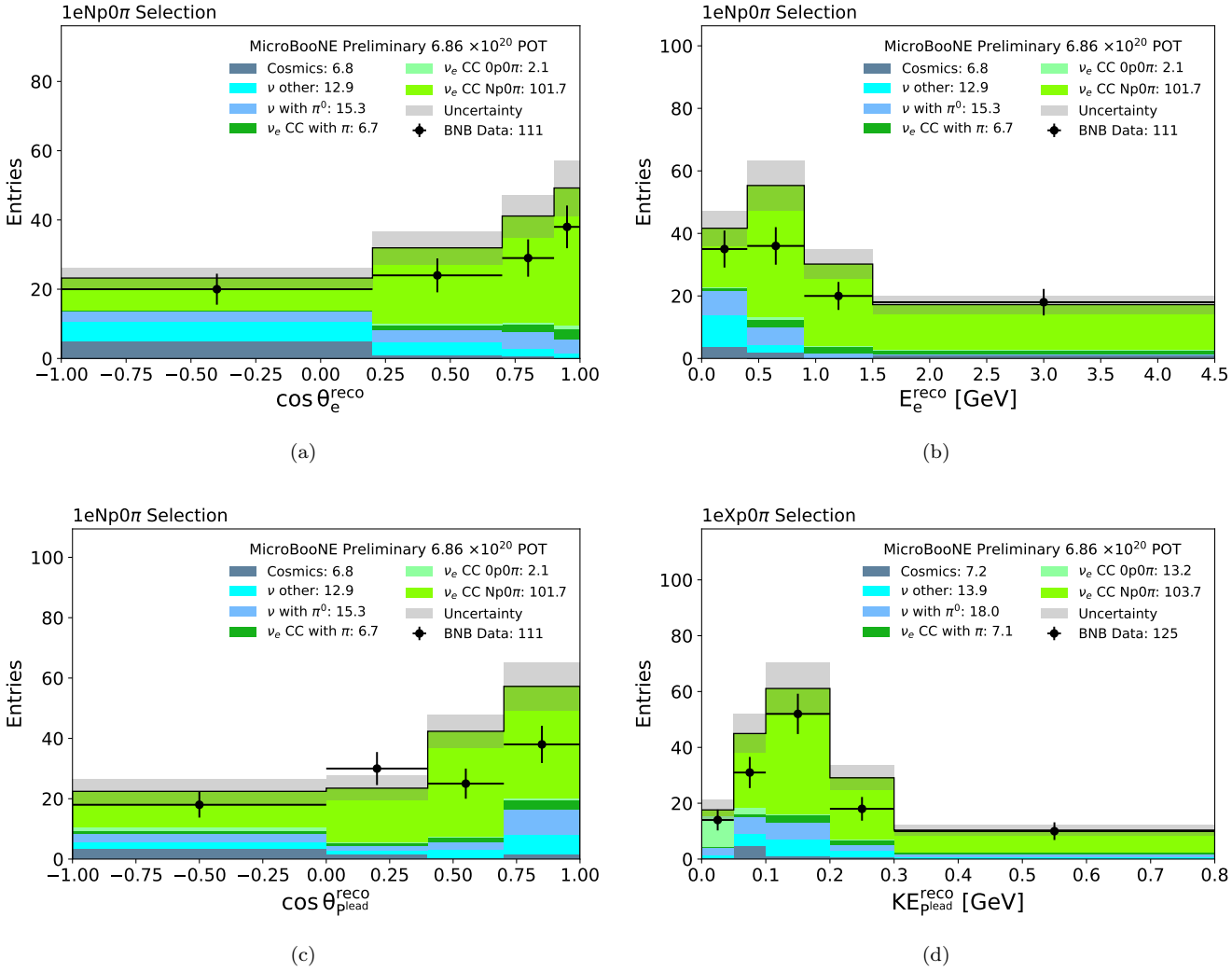

FIG. 1. The observed events in data compared to the MicroBooNE tune of GENIE v3 prediction from simulation. The selection used is reported in each frame. The $1eNp0\pi$ selection is used for (a), (b), (c). The $1eXp0\pi$ = ($1e0p0\pi$ OR $1eNp0\pi$) selection is used for (d), where events selected with the $1e0p0\pi$ selection populate the leftmost bin and events from the $1eNp0\pi$ selection populate the other bins.

Here the covariance matrix is written in terms of bin indices i and j, and constructed as a sum over systematic variations k up until the total number of systematic variations N, with the central value bin content defined as n^{CV} and the content of bin i in variation k defined as n_i^k. Finally, statistical uncertainties from the data measurement are also included as

$$C^{\mathrm{Tot}} = C^{\mathrm{Syst}} + C^{\mathrm{DataStat}},$$

where C^{DataStat} is diagonal with elements corresponding to the Poisson variance in each bin. Statistical uncertainties in the data are the leading source of uncertainty in this measurement.

The observed distributions for the four variables considered in this analysis are shown in Fig. 1, where the data is overlaid on top of the nominal simulation based on the tuned version of GENIE v3 [15]. The simulation tends to over-predict the data, especially at forward angles with respect to the beam and at intermediate energies. These are similar observations to those presented in [3].

In order to extract the cross section from the observed number of events we first define a response matrix, which maps the generated signal events in the true variable space to the observed signal events after selection in the reconstructed space. The off-diagonal elements of the response matrix define the amount of smearing between true

and reconstructed bins. Both $1e0p0\pi$ and $1eNp0\pi$ events are included in the response matrix for the proton energy, with $1e0p0\pi$ events in a single bin and $1eNp0\pi$ events in the other bins. This means that smearing is included between these selections through the off-diagonal elements. Due to the limited size of the selected data sample the bin width is typically larger than the resolution on the measured variables so the fraction of events along the diagonal is >70% across all variables, and >90% for electron angle. A differential cross-section measurement in the true space bin i for the variable x measured in reconstructed space bin j can be defined by the following equation:

$$< \frac{d\sigma}{dx} >_i = \frac{\sum_j R_{ij}^{-1}(N_j - B_j)}{N_{\text{target}} \times \phi \times (\Delta x)_i},$$

where R is the response matrix, N is the number of data events, B is the number of background events, N_{target} is the number of nucleons, and ϕ is the integrated electron neutrino flux. The inversion of the response matrix may lead to instabilities in the cross section results, so we extract the cross section using an unfolding procedure based on the D'Agostini method [36] with three iterations. This number of iterations is found to give results that are stable and with limited bin-to-bin fluctuations. In the cross section extraction, we use a number of nucleons equal to 4.3912×10^{31}, and a POT-integrated BNB ν_e flux of 2.73×10^9 cm^{-2}, which is taken to be the reference flux [37] of the measurement and used as a constant value. As described in a previous MicroBooNE publication [38], this method allows for a more consistent treatment of flux uncertainties.

The resulting cross sections are presented in Fig. 2, where they are compared to a number of modern generators: our nominal tune based on GENIE v3.0.6 [15], GENIE v3.0.6 G18_10a_02_11a [14], GENIE v2.12.2 [39, 40], NuWro 19.02.1 [41, 42], and NEUT v5.4.0 [43, 44]. These generators have different initial state nuclear models (Genie v2 uses a relativistic Fermi gas, while the others use a local Fermi gas), quasi-elastic models (Genie v3 and NEUT use Valencia [45–47], Genie v2 and NuWRO use Llwellyn Smith [48]), and MEC models (Genie v2 uses an empirical model, and the others the Valencia model). Details about the models used in these generators and a more complete description of their differences can be found in other MicroBooNE publications [10, 25, 26] and a summary table presented in [49]. We assess the agreement with these generators by computing χ^2 values and the p-values corresponding to the upper tail of the cumulative distribution for the χ^2 per degrees of freedom. While all generators are in reasonable agreement with the data, the level of agreement differs depending on the generator and the variable. The data indicate a preference for GENIE v3 and NuWro, both of which have a smaller overall prediction. Compared to the plain GENIE v3, the MicroBooNE tune enhances the QE and MEC components and tends to over-predict, especially at intermediate energies. The lowest p-values are obtained for NEUT, which predicts the largest overall cross section, especially at forward proton angles, and GENIE v2, which has the largest prediction for $1e0p0\pi$ events, partly due to its empirical MEC model [50] with no Pauli blocking. The low observed p-values for all generators in the leading proton variable may be affected by a statistical fluctuation inducing migration of data events between the second and third bins.

In summary, this note presents the first differential ν_e-argon cross section measurement without pions in the final state in electron angle and energy as well as leading proton angle and energy, where the proton energy is characterized both above and below the visibility threshold. The findings are typically in agreement with predictions from modern generators, except for tension in the proton angle, with an overall preference for those with lower total cross section. These results may provide input for further tuning of generators, which can potentially improve the ν_e prediction for future new physics searches in MicroBooNE, SBN [51], and DUNE [52]. While this result is statistically limited, an approximately equivalent data set from later run periods remains to be analyzed and can be used, in addition to possible reconstruction and selection improvements, for future cross section analyses.

This document was prepared by the MicroBooNE collaboration using the resources of the Fermi National Accelerator Laboratory (Fermilab), a U.S. Department of Energy, Office of Science, HEP User Facility. Fermilab is managed by Fermi Research Alliance, LLC (FRA), acting under Contract No. DE-AC02-07CH11359. MicroBooNE is supported by the following: the U.S. Department of Energy, Office of Science, Offices of High Energy Physics and Nuclear Physics; the U.S. National Science Foundation; the Swiss National Science Foundation; the Science and Technology Facilities Council (STFC), part of the United Kingdom Research and Innovation; the Royal Society (United Kingdom); and The European Union's Horizon 2020 Marie Sklodowska-Curie Actions. Additional support for the laser calibration system and cosmic ray tagger was provided by the Albert Einstein Center for Fundamental Physics, Bern, Switzerland.

[1] M. Sajjad Athar *et al.*, Prog. Part. Nucl. Phys. **124**, 103947 (2022), arXiv:2111.07586 [hep-ph].
[2] P. Abratenko *et al.* (MicroBooNE), accepted by Phys. Rev. Lett., arXiv:2110.14054 [hep-ex].
[3] P. Abratenko *et al.* (MicroBooNE), (2021), accepted by Phys. Rev. D, arXiv:2110.14065 [hep-ex].
[4] P. Abratenko *et al.* (MicroBooNE), accepted by Phys. Rev. D, arXiv:2110.14080 [hep-ex].

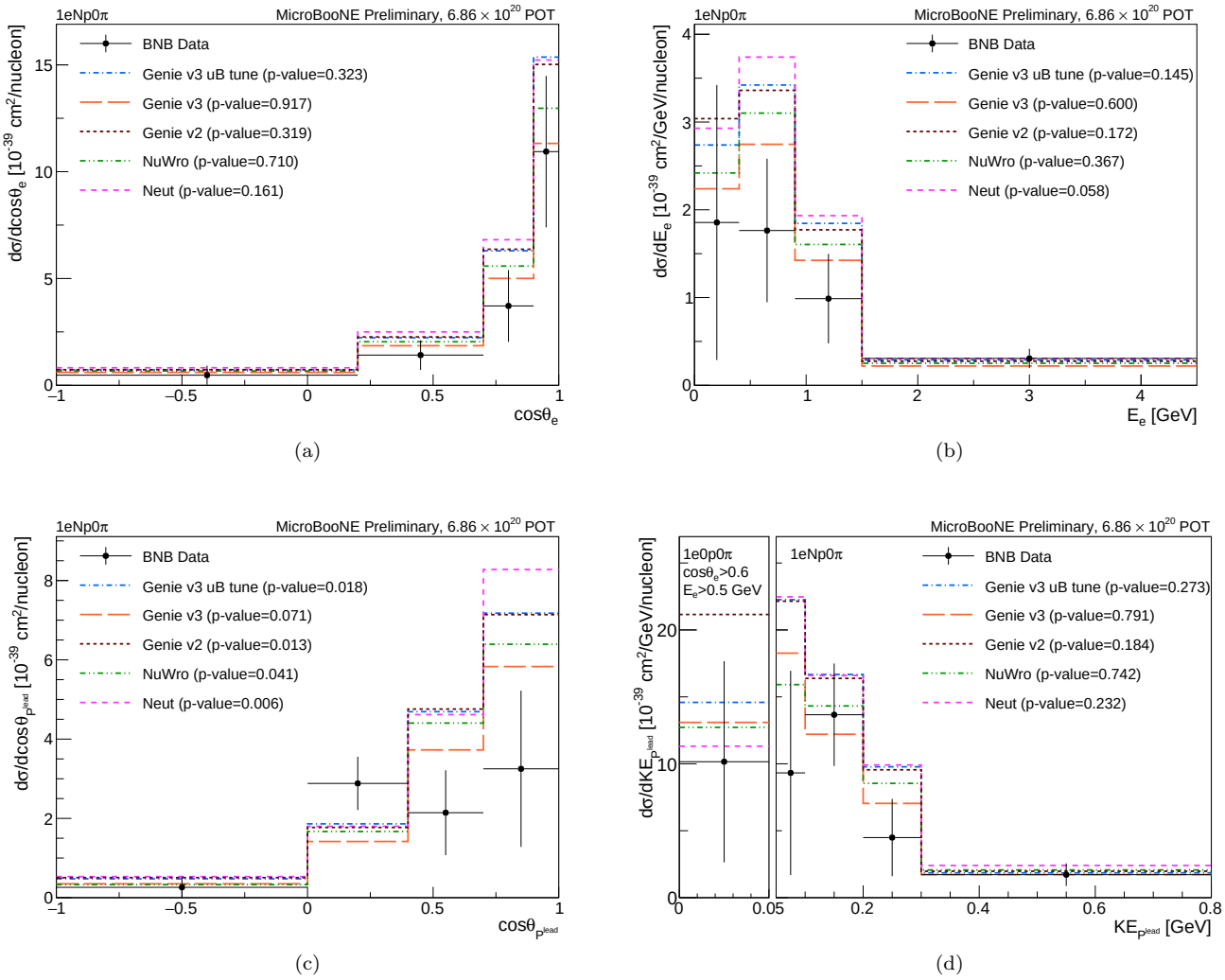

FIG. 2. Unfolded data differential cross section results and comparison with predictions from different generators. The signal definition is reported for each frame: $1eNp0\pi$ is used for (a), (b), (c), and the right frame of (d), while $1e0p0\pi$ with additional phase space restriction is used for the left frame of (d). Compatibility is evaluated in terms of p-values, and reported in the legend.

[5] P. Abratenko *et al.* (MicroBooNE), accepted by Phys. Rev. D, arXiv:2110.13978 [hep-ex].
[6] A. A. Aguilar-Arevalo *et al.* (MiniBooNE), Phys. Rev. D **103**, 052002 (2021).
[7] I. Stancu, FERMILAB-DESIGN-2001-03 (2001), 10.2172/1212167.
[8] R. Acciarri *et al.* (ArgoNeuT), Phys. Rev. D **102**, 011101 (2020).
[9] P. Abratenko *et al.* (MicroBooNE), Phys. Rev. D **104**, 052002 (2021).
[10] P. Abratenko *et al.* (MicroBooNE), Phys. Rev. D **105**, L051102 (2022), arXiv:2109.06832 [hep-ex].
[11] P. Adamson *et al.*, Nucl. Instrum. Meth. A **806**, 279 (2016).
[12] R. Acciarri *et al.* (MicroBooNE), JINST **12**, P02017 (2017).
[13] A. A. Aguilar-Arevalo *et al.* (MiniBooNE), Phys. Rev. D **79**, 072002 (2009).
[14] L. Alvarez-Ruso *et al.* (GENIE), Eur. Phys. J. ST **230**, 4449 (2021), arXiv:2106.09381 [hep-ph].
[15] P. Abratenko *et al.* (MicroBooNE), Phys. Rev. D **105**, 072001 (2022), arXiv:2110.14028 [hep-ex].
[16] S. Agostinelli *et al.* (GEANT4), Nucl. Instrum. Meth. A **506**, 250 (2003).
[17] E. L. Snider and G. Petrillo, J. Phys. Conf. Ser. **898**, 042057 (2017).
[18] C. Adams *et al.* (MicroBooNE), JINST **13**, P07006 (2018).
[19] C. Adams *et al.* (MicroBooNE), JINST **13**, P07007 (2018).
[20] C. Adams *et al.* (MicroBooNE), JINST **15**, P07010 (2020).
[21] P. Abratenko *et al.* (MicroBooNE), JINST **15**, P12037 (2020).
[22] R. Acciarri *et al.* (ArgoNeuT), JINST **8**, P08005 (2013).

[23] R. Acciarri *et al.* (MicroBooNE), Eur. Phys. J. C **78**, 82 (2018).
[24] P. Abratenko *et al.* (MicroBooNE), Phys. Rev. Lett. **128**, 111801 (2022), arXiv:2110.00409 [hep-ex].
[25] P. Abratenko *et al.* (MicroBooNE), Phys. Rev. D **102**, 112013 (2020).
[26] P. Abratenko *et al.* (MicroBooNE), Phys. Rev. Lett. **125**, 201803 (2020).
[27] P. Abratenko *et al.* (MicroBooNE), Phys. Rev. Lett. **123**, 131801 (2019).
[28] C. Adams *et al.* (MicroBooNE), Phys. Rev. D **99**, 091102 (2019).
[29] C. Adams *et al.* (MicroBooNE), Eur. Phys. J. C **79**, 248 (2019).
[30] P. Abratenko *et al.* (MicroBooNE), Phys. Rev. Lett. **127**, 151803 (2021).
[31] P. Abratenko *et al.* (MicroBooNE), Phys. Rev. D **101**, 052001 (2020).
[32] P. Abratenko *et al.* (MicroBooNE), JHEP **12**, 153 (2021), arXiv:2109.02460 [physics.ins-det].
[33] M. Berger, J. Coursey, and M. Zucker (1999) http://physics.nist.gov/Star.
[34] J. Calcutt, C. Thorpe, K. Mahn, and L. Fields, JINST **16**, P08042 (2021).
[35] P. Abratenko *et al.* (MicroBooNE), Eur. Phys. J. C **82**, 454 (2022), arXiv:2111.03556 [hep-ex].
[36] G. D'Agostini (2010) arXiv:1010.0632.
[37] L. Koch and S. Dolan, Phys. Rev. D **102**, 113012 (2020), arXiv:2009.00552 [hep-ex].
[38] P. Abratenko *et al.* ((MicroBooNE Collaboration)*, MicroBooNE), Phys. Rev. Lett. **128**, 151801 (2022), arXiv:2110.14023 [hep-ex].
[39] C. Andreopoulos *et al.*, Nucl. Instrum. Meth. A **614**, 87 (2010), arXiv:0905.2517 [hep-ph].
[40] C. Andreopoulos, C. Barry, S. Dytman, H. Gallagher, T. Golan, R. Hatcher, G. Perdue, and J. Yarba, (2015), arXiv:1510.05494 [hep-ph].
[41] T. Golan, J. T. Sobczyk, and J. Zmuda, Nucl. Phys. B Proc. Suppl. **229-232**, 499 (2012).
[42] T. Golan, C. Juszczak, and J. T. Sobczyk, Phys. Rev. C **86**, 015505 (2012), arXiv:1202.4197 [nucl-th].
[43] Y. Hayato, Acta Phys. Polon. B **40**, 2477 (2009).
[44] Y. Hayato and L. Pickering, Eur. Phys. J. ST **230**, 4469 (2021), arXiv:2106.15809 [hep-ph].
[45] J. Nieves, I. Ruiz Simo, and M. J. Vicente Vacas, Phys. Rev. C **83**, 045501 (2011), arXiv:1102.2777 [hep-ph].
[46] J. Schwehr, D. Cherdack, and R. Gran, (2016), arXiv:1601.02038 [hep-ph].
[47] R. Gran, J. Nieves, F. Sanchez, and M. J. Vicente Vacas, Phys. Rev. D **88**, 113007 (2013), arXiv:1307.8105 [hep-ph].
[48] C. H. Llewellyn Smith, Phys. Rept. **3**, 261 (1972).
[49] D. Doyle *et al.* (NOvA), (2021), arXiv:2109.12220 [hep-ex].
[50] T. Katori, AIP Conf. Proc. **1663**, 030001 (2015), arXiv:1304.6014 [nucl-th].
[51] M. Antonello *et al.* (MicroBooNE, LAr1-ND, ICARUS-WA104), arXiv:1503.01520 [physics.ins-det].
[52] B. Abi *et al.* (DUNE), (2020), arXiv:2002.03005 [hep-ex].

Appendix A: Supplementary Material

1. Proton Threshold

The choice of the proton threshold at 50 MeV is motivated by Fig. 3, where we show the expected number of selected signal events as a function of the true leading proton kinetic energy for the $1e0p0\pi$ and $1eNp0\pi$ selections. The choice of 50 MeV corresponds to the energy where the two curves intersect, so below (above) this value most events are selected with the $1e0p0\pi$ ($1eNp0\pi$) selection.

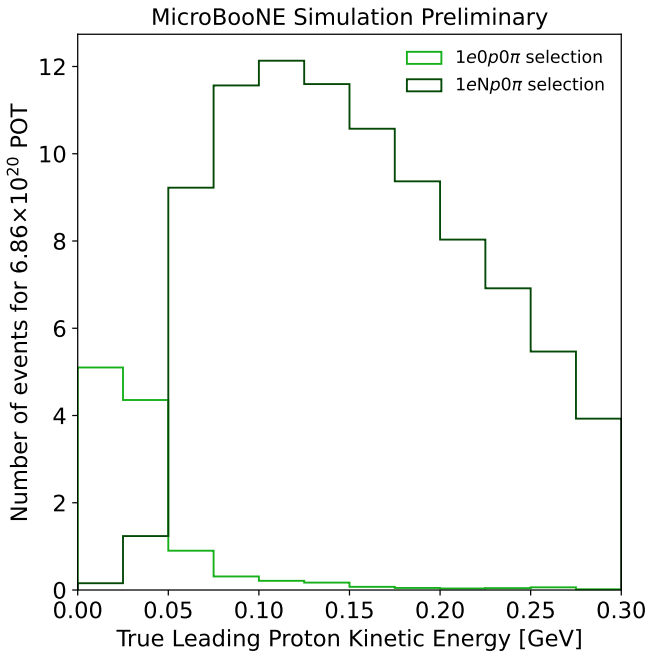

FIG. 3. Expected number of signal events for 6.86×10^{20} POT as a function of the leading proton kinetic energy, for the $1e0p0\pi$ and $1eNp0\pi$ selections.

2. Additional plots

The BDT score used to select electron neutrinos at the stage before th BDT cut is made is shown in Fig 4.

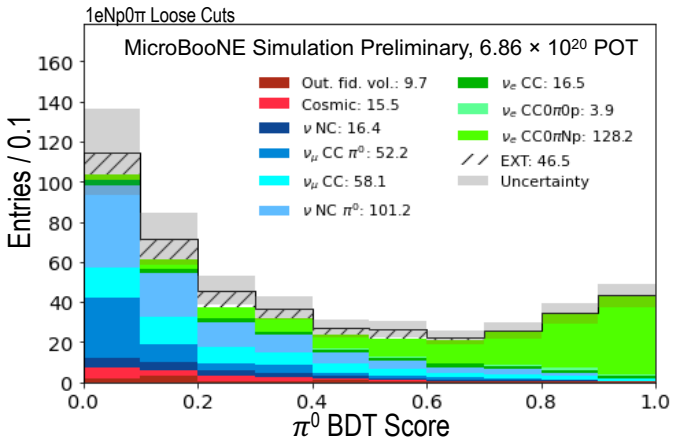

FIG. 4. BDT score used to select electron neutrinos at an intermediate selection stage, referred to as the "Loose Cuts". The BDT training in this figure comes from [3].

The systematic uncertainties on the selected electron neutrino events are shown in bins of electron angle relative to the neutrino beam in Fig. 5.

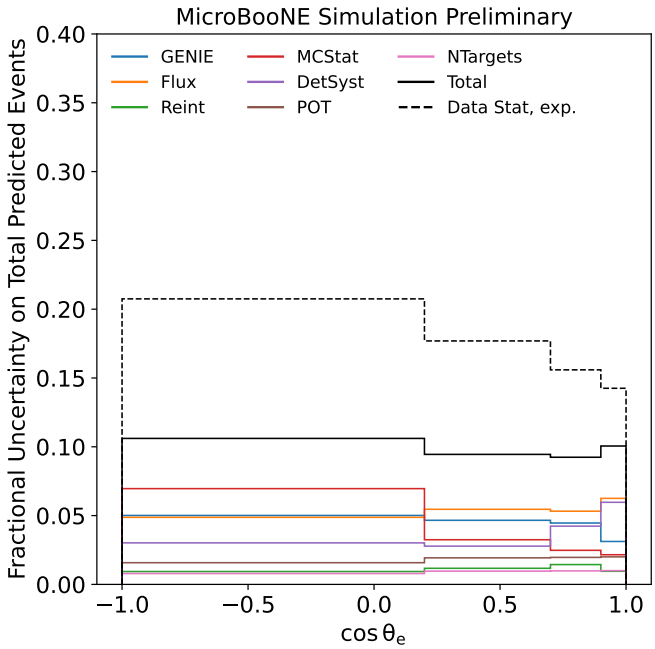

FIG. 5. Systematic uncertainty breakdown on the number of predicted events in bins of electron angle relative to the neutrino beam.

The response matrix from true electron angle to reconstructed electron angle is shown in Fig. 6.

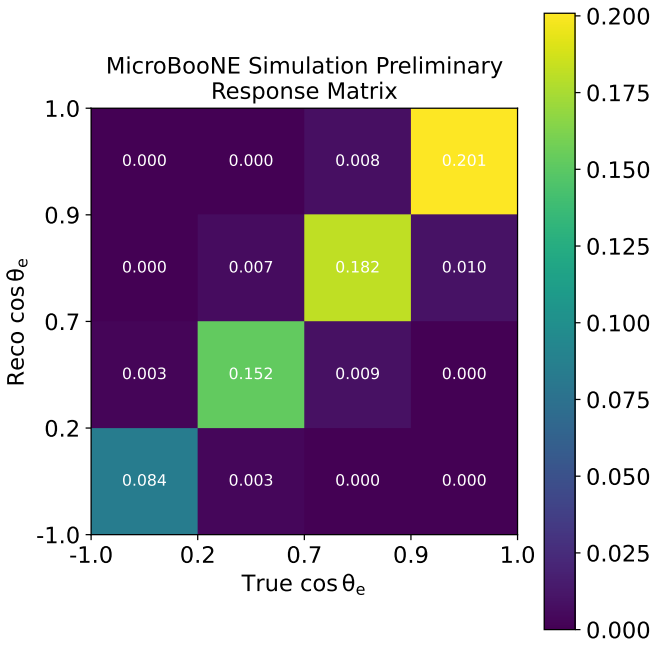

FIG. 6. Response matrix in electron angle relative to the neutrino beam.